THE JOURNAL OF PHYSICAL CHEMISTRY B

Article

pubs.acs.org/JPCB

# Theoretical Study of Raman Spectra of Methanol in Aqueous Solutions: Non-Coincident Effect of the CO Stretch

Yuanyuan Sun, Renhui Zheng, and Qiang Shi*

Beijing National Laboratory for Molecular Sciences, State Key Laboratory for Structural Chemistry of Unstable and Stable Species, Institute of Chemistry, Chinese Academy of Sciences, Zhongguancun, Beijing 100190, China

**ABSTRACT:** Raman spectra of the CO stretch for liquid methanol and its aqueous solutions were simulated using the combined electronic structure and molecular dynamics simulation method. The instantaneous vibrational frequencies were obtained from an empirical mapping to the electrostatic potentials, while vibrational couplings between different molecules were calculated using the transition dipole coupling model. It is found that noncoincident effects (NCEs) at high concentrations are dominated by the intermolecular couplings of CO stretch and decrease monotonically as the methanol concentration decreases. This behavior is explained as the effect of reduced methanol−methanol hydrogen bonding with the addition of water. A non-monotonic change of the NCEs defined by the peak position of the CO stretch as a function of methanol mole fraction is found, which is ascribed to band asymmetry caused by reorientational dynamics.

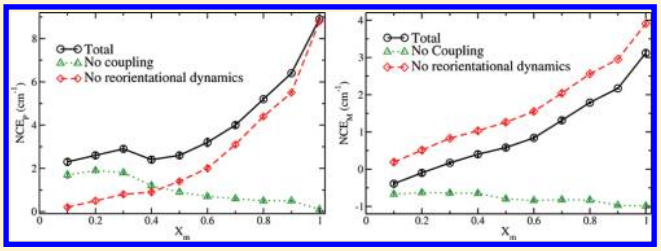


## INTRODUCTION

Methanol−water mixtures, as a model system for aqueous solutions of alcohols, have been extensively studied both experimentally[1−7] and theoretically.[8−13] Methanol and water are both hydrogen-bonding liquids, but the minor difference in their molecular structures leads to apparent differences in liquid phase structures: Water molecules form the well-known tetrahedral-like three-dimensional networks, whereas methanol molecules are bound into local structures consisting of chains, rings, or small clusters.[2,3,14−16] Methanol is soluble to water in any proportion. However, they are incompletely mixed at the microscopic scale: the hydrophobic methyl groups tend to be pushed together and away from water, while the hydrophilic OH groups of methanol molecules are hydrogen bonded to the surrounding water molecules.[3] When the methanol mole fraction changes, the microscopic structure also varies. As a consequence, methanol−water mixtures often show anomalous properties relative to those of the pure components. For example, the excess mixing enthalpy[8,17] and the self-diffusion constants[8,18,19] vary non-monotonically as a function of methanol mole fraction.

Structural information of methanol/water mixtures can be obtained from neutron diffraction,[1,3,4] X-ray emission spectroscopy,[2] dielectric relaxation measurements,[5] and molecular dynamics simulations.[8,9] On the basis of these studies, different structural models were proposed to explain the anomalous properties of methanol/water mixtures. The traditional model from early neutron diffraction experiments is that the microstructure of water is enhanced in the presence of methanol, and the water molecules form ice-like cages surrounding the methyl groups of methanol.[4,20] This assumption has been challenged by the new neutron diffraction experiment,[3] which suggests that methanol and water form separate bipercolating hydrogen-bonded networks. This model is also supported by molecular dynamics simulations in order to interpret the non-monotonic dependence of the excess mixing enthalpy and the self-diffusion constant on methanol concentration.[1] More recently, results from X-ray scattering provide a new explanation for the entropy decrease due to water molecules bridging chains of six or eight methanols to form rings.[2]

Spectroscopy measurements play an important role in studying the structures and dynamics of liquids. The IR and Raman spectra of liquid methanol[21−23] and methanol−water mixtures[6,7,24,25] were studied to investigate the couplings of the vibrational motions between different molecules. The optical Kerr spectroscopy has also been used to study reorientational dynamics in liquid methanol.[26,27] In the Raman spectra studies of the methanol−water mixtures, Zerda et al. reported how the noncoincident effect (NCE) between anisotropic and isotropic Raman profiles of CO stretch in methanol changes with the mole fraction of methanol $X_m$ in methanol−water mixtures.[6] Their conclusion is that the splitting decreases with dilution apparently due to the local order disturbed by water molecules. Similar results were obtained by Dixit et al.[24] Raman spectra studies were also performed for methanol molecules in the nonpolar solvent $CCl_4$,[28,29] where the NCE of CO stretch was found to increase upon dilution with $CCl_4$ at low concentrations.

In this paper, we calculated the NCE of CO vibration as a function of the methanol mole fraction, using the combined electronic structure/molecular dynamics (ES/MD) simulation

**Received:** January 6, 2012
**Revised:** March 20, 2012
**Published:** March 23, 2012

 © 2012 American Chemical Society  dx.doi.org/10.1021/jp300178v | J. Phys. Chem. B 2012, 116, 4543−4551

method.[30−34] The ES/MD method employs the mixed quantum and classical method originally motivated by the Kubo−Anderson theory of line shapes.[35,36] In this method, the high frequency vibrational modes are treated quantum mechanically, while the effects of the other degrees of freedom are treated as stochastic modulations of the vibrational frequencies and couplings. In recent studies, the ES/MD method has been successfully applied in calculating linear, nonlinear spectra in liquid water,[30−34,37] as well as vibrational sum-frequency spectra at the water/air interfaces.[38,39] In a previous work,[40] we calculated the infrared and Raman spectra of the OH stretches in liquid methanol using the ES/MD approach, and found reasonable agreement with experiments. In this paper, the same approach is applied to calculate the Raman spectra of CO vibration in methanol and methanol−water mixtures, and to investigate the NCE as a function of the methanol mole fraction.

The remainder of this paper is arranged as follows. In section II, theoretical methods for calculating the Raman spectra are presented; in section III, the ES/MD method is used to calculate the Raman spectra and the NCEs of methanol−water mixtures, and to explain the experimental findings; the conclusions and discussions are made in section IV.

## THEORETICAL METHODS

Raman spectra in liquids can be calculated from the quantum time-correlation functions (TCFs).[32,40−42] In a Raman experiment, if the incident light is polarized in the $\hat{\varepsilon}_0$ direction and the scattered beam is detected in the $\hat{\varepsilon}_s$ direction, then the Raman spectra can be written as

$$I(\omega) \sim \mathrm{Re} \int_0^\infty \mathrm{d}t\ \mathrm{e}^{-i\omega t}\langle \hat{\varepsilon}_0\cdot\alpha(0)\cdot\hat{\varepsilon}_s\hat{\varepsilon}_0\cdot\alpha(t)\cdot\hat{\varepsilon}_s\rangle \tag{1}$$

where Re is the real part of the integral and $\alpha$ is the transition polarizability tensor operator of the system.

In the mixed quantum and classical dynamics simulations, the CO stretches of methanol are treated quantum mechanically, while other degrees of freedom are treated classically using MD simulation.[31,43−48] Under the above assumptions, eq 1 can be calculated as[44]

$$I(\omega) \sim \mathrm{Re} \int_0^\infty \mathrm{d}t\ \mathrm{e}^{-i\omega t} \sum_{ij} \langle \alpha_{ipq}(0)F_{ij}(t)\alpha_{jpq}(t)\rangle \mathrm{e}^{-t/2T_1} \tag{2}$$

where $\alpha_{ipq}$ is the polarizability tensor of the $i$th molecule, $T_1$ is the lifetime of vibrational excitation, and $p$ and $q$ denote the laboratory-fixed frame $X$, $Y$, or $Z$ axes. If the polarization of the scattered beam is parallel to that of the incident light ($p = q$), it is referred to as the parallel-polarized (VV) spectra. On the other hand, if the polarization of the scattered beam is perpendicular to that of the incident light ($p \neq q$), it is referred to as the perpendicular-polarized (VH) spectra. $F_{ij}(t)$ is the element of the time-dependent matrix $F(t)$, satisfying the following equation

$$\frac{\mathrm{d}F(t)}{\mathrm{d}t} = iF(t)\Omega(t) \tag{3}$$

with the initial condition that $F_{ij}(0) = \delta_{ij}$, and

$$\Omega_{ij}(t) = \omega_i(t)\delta_{ij} + \omega_{ij}(t)(1 - \delta_{ij}) \tag{4}$$

Here, the diagonal elements of the matrix $\Omega(t)$ are the fluctuating transition frequencies of each molecule at time $t$, while the off-diagonal elements are the vibrational couplings between different molecules. In this study, the instantaneous transition frequencies are modeled using an electrostatic potential-based frequency mapping scheme detailed in the next section. The vibrational coupling between different molecules are calculated using the transition dipole coupling (TDC) model[49−52] and expressed as[53]

$$\hbar\omega_{ij} = \frac{|\partial\mu_i/\partial Q_i|\cdot|\partial\mu_j/\partial Q_j|S_iS_j}{r_{ij}^3} \times \{\hat{u}_i\cdot\hat{u}_j - 3[(\hat{u}_i\cdot\hat{n}_{ij})\cdot(\hat{u}_j\cdot\hat{n}_{ij})]\} \tag{5}$$

where $S_i = \langle 0|Q_i|1\rangle = (\hbar/2\omega_i)^{1/2}$ is the expectation value of the normal coordinate $Q_i$ between vibrational eigenstates $|0\rangle$ and $|1\rangle$, $\hat{n}_{ij}$ is the unit vector along the line connecting the two dipoles, and $r_{ij}$ is the distance between them; $\partial\mu_i/\partial Q_i$ is the derivative of the transition dipole of the $i$th molecule; $\hat{u}_i$ is the unit vector along the CO bond of the $i$th molecule. The placement of the transition dipole was found to affect the calculation of the transition-dipole couplings.[32] In our work, the transition dipole is placed on the middle point of the CO bond.

Calculation of the transition polarizability for each molecule is essential for simulating Raman line shapes. In this study, the bond polarizability model is employed, where the Raman tensor of each molecule is assumed to be axially symmetric with respect to the bond of interest (i.e., the CO bond); the $pq$ component of the transition polarizability tensor is then given by[33,54]

$$\alpha_{pq} = S_{10}[(\alpha'_{\parallel} - \alpha'_{\perp})(\hat{u}\cdot\hat{p})(\hat{u}\cdot\hat{q}) + \alpha'_{\perp}(\hat{p}\cdot\hat{q})] \tag{6}$$

where $\alpha'_{\parallel}$ and $\alpha'_{\perp}$ are the parallel and perpendicular bond-polarizability derivatives, respectively; $S_{10} = (\hbar/2\omega_{CO})^{1/2}$ is the 0−1 matrix of the CO stretch coordinate; $\hat{u}$ is the unit vector along the CO bond.

The isotropic and anisotropic components of the Raman spectra are also frequently used in the literature, which can be obtained from the VV and VH components as[28]

$$I_{ani}(\omega) = I_{VH}(\omega)$$
$$I_{iso}(\omega) = I_{VV}(\omega) - \frac{4}{3}I_{VH}(\omega) \tag{7}$$

## RESULTS

**The Instantaneous Transition Frequencies.** The local environment causes shift and fluctuation of the CO stretch frequency in solution. In the literature, different empirical mapping schemes were proposed to calculate the instantaneous vibrational transition frequency of a molecule from its environment.[32,40,43,55−60] We have used the electrostatic-potential-based frequency mapping scheme that was used in several recent studies.[57−60] Here, the instantaneous vibrational frequencies are modeled as a linear function of electrostatic potentials on specific sites on the molecule.

To find the empirical relation between the vibrational frequencies of the CO stretch and the electrostatic potentials, *ab initio* calculations were first performed. Random clusters of a solute molecule and the surrounding solvent molecules were first chosen from a MD simulation, where both the solvent and solute are $CH_3OH$. Fifty such clusters were generated by the following scheme: (1) The O atom of a methanol molecule in the simulation was first selected to define the CO bond of


dx.doi.org/10.1021/jp300178v | J. Phys. Chem. B 2012, 116, 4543−4551

interest. (2) Any molecule with its oxygen atom within 5 Å of the selected oxygen was included in the cluster. (3) Other molecules having their oxygen within 9 Å of the selected oxygen were included as point charges. We then calculated the CO vibrational frequencies for the target molecule in these sampled clusters using *ab initio* calculations. This was done by fully optimizing the target molecule with other nuclei fixed at the B3LYP/6-31+G* level using the Gaussian 03 software package.[61] The calculated vibrational frequencies were used for the fitting without any rescaling.

To give a better fit of the instantaneous CO stretch frequencies, we adopted a nine-site model considering electrostatic potentials at the six atomic sites of the methanol molecule, and three additional sites around the oxygen atom illustrated in Figure 1. One extra site was located at 0.7 Å away

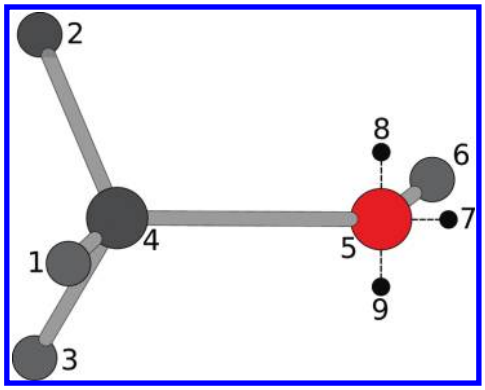


**Figure 1.** Nine interaction sites used for the empirical mapping of the CO stretch frequency in eq 9.

from the oxygen atom along the CO bond. The other two were symmetrically placed on the line passing through the oxygen atom and perpendicular to the HCOH plane. Their distances from the oxygen atom were also 0.7 Å. The electrostatic potential $\phi_i$ at the $i$th site was calculated from the surrounding partial charges as

$$\phi_i = \frac{1}{4\pi\varepsilon_0} \sum_m \sum_j \frac{q_j^m}{r_{ij}^m} \tag{8}$$

where $q_j^m$ denotes the partial charge of the $j$th site of the $m$th methanol molecule and $r_{ij}^m$ is the distance between the $i$th and the $j$th site of the $m$th methanol molecule.

The CO stretch frequencies from the *ab initio* calculation were then fitted to a linear function of the electrostatic potentials

$$\omega = \omega_0 + \sum_{i=1}^{9} l_i \phi_i \tag{9}$$

where $\omega_0$ is the frequency in a vacuum and $l_i$ is the expansion coefficient on the $i$th site. The units of $\omega$ is $cm^{-1}$, and the electrostatic potential $\phi_i$ is in atomic units. Because of the symmetry of the interaction sites, we have also assumed that $l_2 = l_3$ and $l_8 = l_9$. The parameters were also constrained by the relation $\sum_{i=1}^{9} l_i = 0$. With this constraint, there are seven independent parameters (including $\omega_0$), and the above equation can be rewritten as

$$\omega = \omega_0 + \sum_{i=1}^{8} l_i(\phi_i - \phi_9) \tag{10}$$

A linear least-squares fitting with eq 10 was performed to determine $\omega_0$ and $l_i$ ($i$ = 1−8). The $\omega_0$ value is 1065.7 $cm^{-1}$. The $l_1$−$l_3$ values representing the sites on the three hydrogen atoms attached to the C atom are 289.5, 773.6, and 773.6, respectively. The $l_4$−$l_6$ values representing the sites on the C atom, O atom, and H atom are −1093.7, −384.1, and −134.1, respectively. The parameter $l_7$ for the site along the CO bond is 674.6, while the parameters $l_8$ and $l_9$ for the two sites perpendicular to the HCOH plane are −449.7. The correlation coefficient is 0.85. The CO frequencies calculated by eq 10 were compared with DFT calculated frequencies in Figure 2.

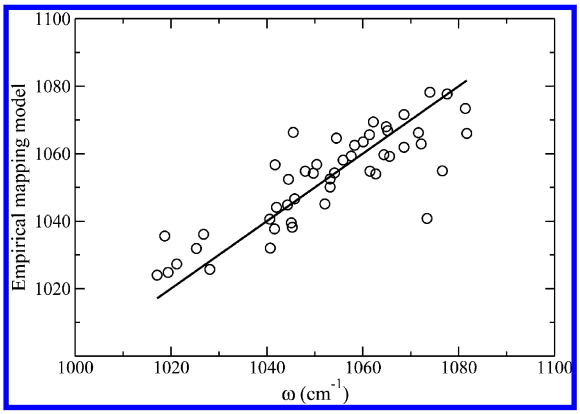


**Figure 2.** CO stretch frequencies calculated with the electrostatic potential-based mapping using eq 10 vs frequencies calculated using DFT.

We note that the standard deviation of the fitting is around 15 $cm^{-1}$. This should have some effect on the calculated line widths but should have little influence on the NCEs.

**Molecular Dynamics Simulations.** MD simulations of liquid methanol and methanol−water mixtures were performed using the OPLS-AA force field[62] at a temperature of 298.15 K with the DL_POLY program.[63] The total number of molecules in the simulation box is 250 with the methanol mole fraction changing from 0.1 to 1 in 0.1 increments. Periodic boundary conditions were employed, and the long-range electrostatic interactions were calculated by the Ewald summation.[64] The classical equations of motion were integrated with the leapfrog algorithm[65] with a time step of 1 fs. The system was first equilibrated using NPT simulation for 2 ns with the reference pressure set to 1 atm, whereafter NVT simulation was employed to generate the trajectories for Raman spectra calculation.

Radial distribution functions (RDFs) provide an averaged picture of the surroundings of each molecule. We computed the methanol O−methanol O ($O_m$−$O_m$), methanol O−water O ($O_m$−$O_w$), and methanol C−methanol C (C−C) RDFs. The results are shown in Figure 3, which agree with previous theoretical studies.[1,8] The integrated coordination numbers for all concentrations were also calculated, and their values at 3.2 Å for $g_{O_mO_m}(r)$, 3.2 Å for $g_{O_mO_w}(r)$, and 6.0 Å for $g_{CC}(r)$ are shown in Figure 4, which correspond to the number of atoms in the first solvation shell. It can be seen that there are significant changes of the $O_mO_m$ RDFs: the first solvation shell peak becomes smaller and broader as the methanol concentration


dx.doi.org/10.1021/jp300178v | J. Phys. Chem. B 2012, 116, 4543−4551

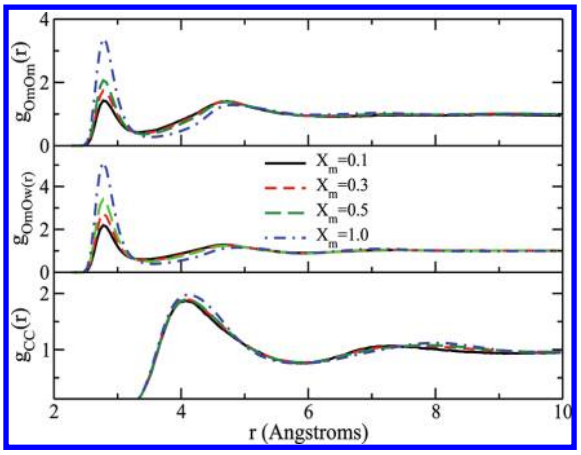


**Figure 3.** Calculated methanol O−methanol O, methanol O−water O, and methanol C−methanol C radial distribution functions at different methanol concentrations (the blue dash-dotted line represents $X_m$ = 0.9 for $g_{O_mO_w}(r)$ in the middle panel).

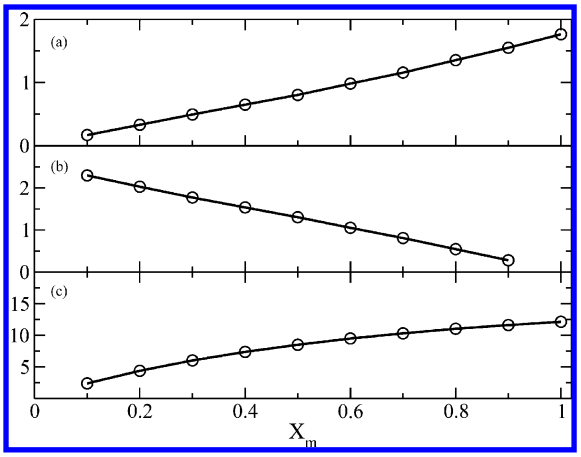


**Figure 4.** The integrated coordination numbers in the first solvation shell at different methanol concentrations for (a) $g_{O_mO_m}(r)$, (b) $g_{O_mO_w}(r)$, and (c) $g_{CC}(r)$.

decreases. In pure methanol liquid, most molecules form two hydrogen bonds in the form of chains, so that the average number of $O_m$ atoms in the first solvation shell is around 2.0. This number decreases with the decrease of $X_m$, approximately as a linear function of $X_m$, with slight deviations at small $X_m$. The average number of water O atoms in the first solvation shell of a methanol O atom increases to about 2.5 for dilute solutions, indicating that a methanol molecule forms around 2−3 hydrogen bonds with water molecules.

In contrast to the $O_mO_m$ RDFs, the C−C RDFs do not change significantly for the first solvation shell, except for slight shifts of the first peak toward a shorter distance with reduced methanol concentration. However, there are significant shifts of the peaks of the second C−C solvation shell toward shorter distances as $X_m$ decreases. This can be understood as that the first C−C solvation shell is formed due to direct methanol−methanol interactions, while, at low concentrations, the second solvation shell is mainly related to the interaction of two methanol molecules with the same water molecule. The integrated coordination number in the first solvation shell (defined as $r$ < 6.0 Å) shows that, even at $X_m$ = 0.1, 2−3 methanol molecules are still present in the first solvation shell of the CC peak. However, on the basis of the C−C RDFs, there is no significant congregation of the methyl groups in the methanol−water mixtures.

To characterize the methanol−methanol hydrogen bonding, we calculated the average methanol−methanol hydrogen-bond number of methanol molecules in methanol−water mixtures. When the intermolecular O···O distance of two methanol molecules is smaller than 3.5 Å and the angle O−H···O is larger than 150°, the two molecules are hydrogen-bonded.[66] The total numbers of the methanol−methanol hydrogen bonds in different methanol−water mixtures were calculated, and the average hydrogen-bond number is defined as the total number of methanol−methanol hydrogen bonds divided by the total number of methanol molecules. Since the methanol molecules usually form chains in liquids, this number is less than 1. We plot the average hydrogen-bond number as a function of the methanol concentration in Figure 5. A monotonic decrease of

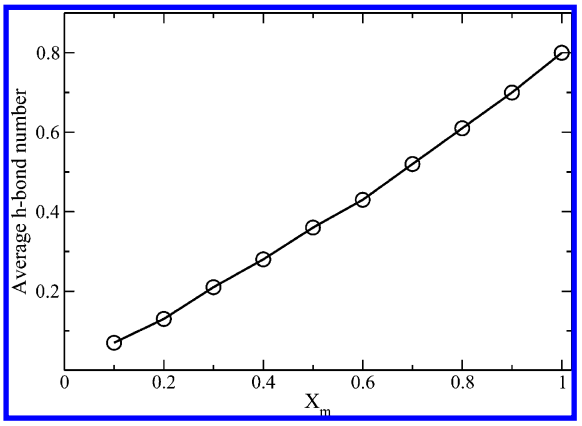


**Figure 5.** Average methanol−methanol hydrogen-bond number defined as the total number of methanol−methanol hydrogen bonds divided by the total number of methanol molecules, as a function of the methanol fraction.

the average number of methanol−methanol hydrogen bonds as a function of $X_m$ is found. At low concentrations ($X_m$ < 0.5), the average hydrogen-bond number deviates slightly from the linear function of $X_m$, which is also consistent with the integrated $O_mO_m$ RDFs in Figure 4. As the consequence of reduced methanol−methanol hydrogen bonding, the long methanol chains will break into smaller ones as more water is added. This trend is shown in Figure 6, where the distributions of the length

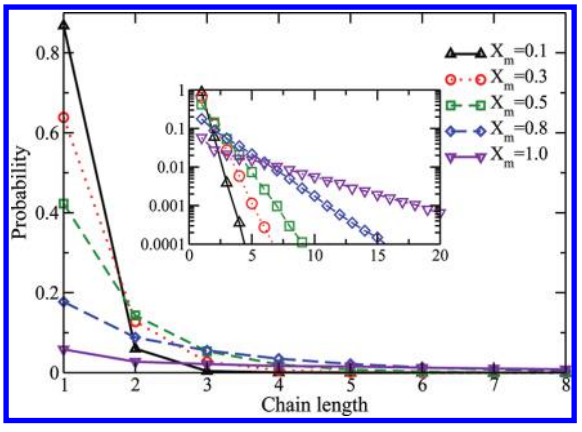


**Figure 6.** Distributions of the lengths of hydrogen-bonded methanol chains in liquid methanol and methanol−water mixtures.


dx.doi.org/10.1021/jp300178v | J. Phys. Chem. B 2012, 116, 4543−4551

of hydrogen-bonded methanol chains at different methanol concentrations are shown.

The electrostatic potentials at the nine sites on each methanol molecule were first calculated, using the molecules that would be chosen for a DFT cluster calculation, as described in section III. The CO stretch frequencies $\omega_i$ were then obtained using the mapping relation in eq 10, and the intermolecular coupling frequencies $\omega_{ij}$ were computed using eq 5. In Figure 7, we plot the distribution of CO vibrational

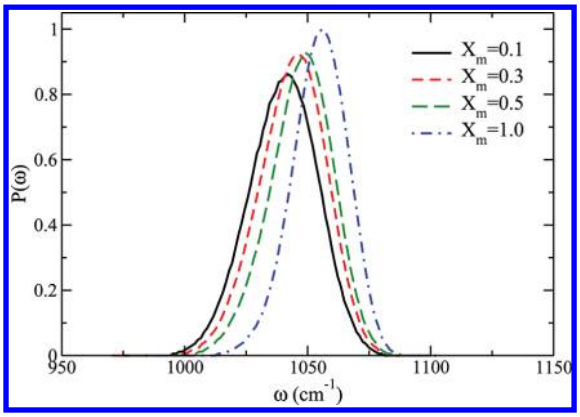


**Figure 7.** Frequency distributions of CO stretch in liquid methanol and methanol–water mixtures.

frequencies at several methanol mole fractions. It can be seen that the peaks of the frequency distributions shift from 1056 $cm^{-1}$ ($X_m$ = 1.0) to 1042 $cm^{-1}$ ($X_m$ = 0.1), while the width of the distribution changes from 28 $cm^{-1}$ ($X_m$ = 1.0) to 38 $cm^{-1}$ ($X_m$ = 0.1). The time-correlation function of vibrational frequencies is calculated as

$$C(t) = \langle \delta\omega_i(t)\delta\omega_i(0)\rangle \quad (11)$$

where $\delta\omega_i(t)$ is the difference between the vibrational frequency $\omega_i(t)$ and the average frequency $\langle\omega\rangle$. The normalized frequency correlation functions are plotted in Figure 8 for several

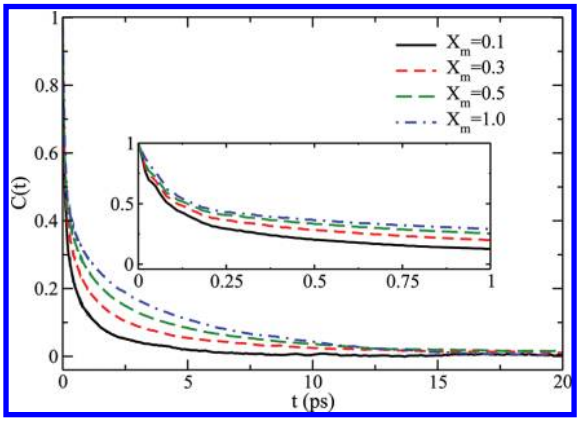


**Figure 8.** Frequency autocorrelation functions of CO stretch in liquid methanol and methanol–water mixtures.

methanol concentrations. We can see that $C(t)$ shows dynamics at different time scales: for example, there is a fast decay of 80 fs and slower decays of 1.0 and 8.0 ps in pure methanol. The existence of both fast and slower time scales indicates that the vibrational spectra will show features of both inhomogeneous broadening and motional narrowing.

We have also calculated the distributions of intermolecular couplings $\omega_{ij}$ between different methanol molecules at different concentrations. The results are shown in Figure 9. The

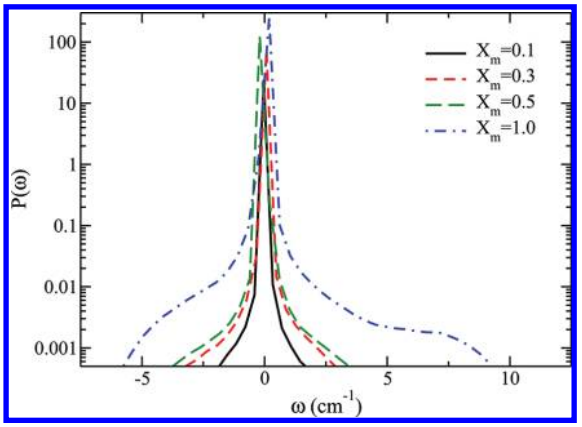


**Figure 9.** Distributions of intermolecular couplings of methanol molecules in liquid methanol and methanol–water mixtures.

distribution is normalized such that the integrated number of couplings is equal to $N - 1$, where $N$ is the number of methanol molecules in the simulation box. It can be seen that, with the decrease of the methanol concentration, couplings between molecules decrease. We note that the strongest intermolecular couplings which correspond to the tails of Figure 9 should come from the nearest neighbor in the hydrogen-bonded methanol chains. Thus, the decrease of intermolecular couplings is consistent with the decrease of methanol–methanol hydrogen bonding in Figure 5.

**Raman Spectra of CO Stretch in Methanol–Water Mixtures.** Raman spectra were calculated for liquid methanol and methanol–water mixtures using eqs 2–4. In this work, we have found that the transition dipole derivatives and polarizability tensor derivatives are not as sensitive to the environmental electronic fields as in our previous studies of the OH spectra.[40] Thus, we have neglected the non-Condon effects in calculating the Raman spectra. The ratio $\alpha'_{\parallel}/\alpha'_{\perp}$ is set to be 22 to reproduce the depolarization ratio of 0.28 from the gas phase DFT calculation. The VV and VH components were first obtained, and the isotropic and anisotropic components were then calculated using eq 7. Short trajectory segments were selected from a long simulation to calculate the Raman spectra. The length of each trajectory segment is 4 ps, and the time interval between consecutive segments is 1 ns. Converged spectra were obtained by averaging over 20 ($X_m$ = 1.0), 100 ($0.6 \le X_m \le 0.9$), and 200 ($X_m \le 0.5$) trajectory segments.

The calculated Raman spectra for pure methanol are plotted in Figure 10. The CO stretch lifetime in pure methanol is not available in the literature. In calculating the spectra, the population relaxation time was set to be $T_1$ = 3.2 ps, which is the CO stretch lifetime for methanol in liquid carbon tetrachloride.[67] The calculated isotropic Raman spectra peak is located at 1060.0 $cm^{-1}$ with a FWHM of 19.2 $cm^{-1}$, while the peak of anisotropic Raman spectra is located at 1051.1 $cm^{-1}$ with a FWHM of 34.6 $cm^{-1}$, leading to a NCE of −8.9 $cm^{-1}$. The peak positions are larger than the experimental ones[6,28,29] by about 20 $cm^{-1}$, which should be due to the inaccuracy of the DFT calculation of the vibrational frequencies. The isotropic and anisotropic components of the Raman spectra of CO stretch of pure methanol liquid have been studied exper-


dx.doi.org/10.1021/jp300178v | J. Phys. Chem. B 2012, 116, 4543–4551

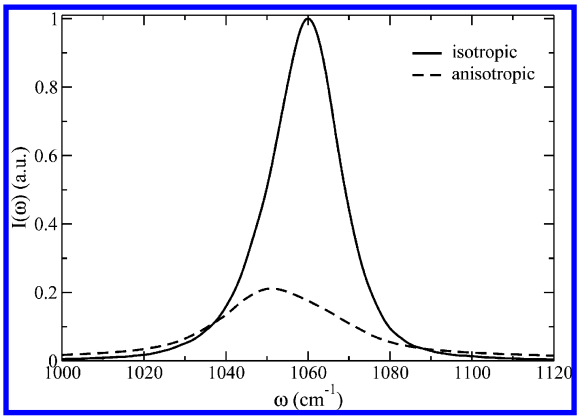


**Figure 10.** Calculated Raman isotropic (solid line) and anisotropic (dashed line) spectra for pure liquid methanol.

imentally.[6,28,29] The NCE values from these studies are −5.1,[6] −6.3,[29] and −7.3 cm$^{-1}$.[28] The FWHMs of isotropic and anisotropic peaks from experimental studies are 22.5 and 29.4 cm$^{-1}$, respectively.[28,68] Therefore, the theoretical NCE for pure methanol liquid is slightly smaller than the experimental values, and the FWHMs agree reasonably well with experimental results.

The VV and VH peak positions at different concentrations were plotted in Figure 11, and compared with the experimental

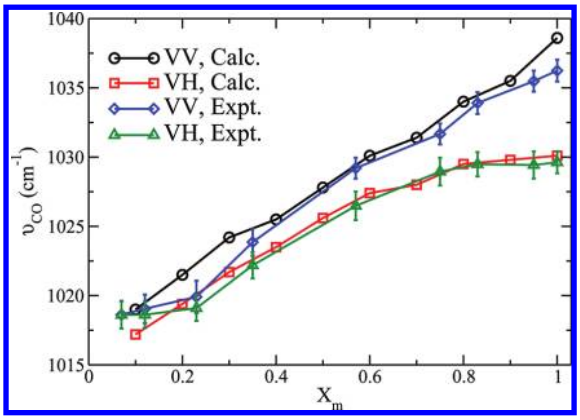


**Figure 11.** Calculated Raman VV and VH peak positions, in comparison with the experimental results from ref 24. The calculated results are shifted by −21 cm$^{-1}$ for a better comparison. Error bars for the calculated results are less than the size of the symbols.

result from ref 24. The calculated peak positions are shifted by −21 cm$^{-1}$ for a better comparison. It can be seen that the calculated changes of peak positions agree well with the experimental results. Especially, the nonlinear change of the VH peak positions at high methanol concentration is well reproduced in the calculations.

The concentration dependence of the NCEs for CO stretch in methanol−water mixtures is depicted in Figure 12 as the solid curve. To calculate the error bars shown in Figure 12, the trajectory segments were first divided into five groups. NCE values were then obtained by calculating the Raman spectra from each group of trajectory segments. Finally, the standard deviation of the five NCE values was used to estimate the error bars. When the concentration dependent NCE is studied, the NCE is defined as the isotropic peak position minus the anisotropic peak position. The results mearsured by peak

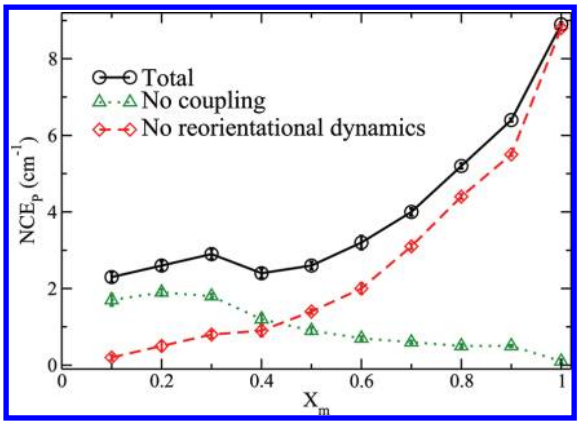


**Figure 12.** Concentration dependence of NCE of CO stretch measured by peak positions in liquid methanol and methanol−water mixtures.

positions show that, when water is added in methanol, the peak splitting between the isotropic and anisotropic components decreases. This is consistent with the changes of VV and VH peak positions found in ref 24. For methanol mole fraction $X_m$ < 0.4, there is an increase of the NCE until $X_m$ < 0.3. In low concentrations $X_m$ < 0.3, the NCE decreases again. This feature of non-monotonic change of NCE can not be seen in the experimental results in ref 24; part of the reason could be due to the large standard deviation of the peak positions. We note that this behavior agrees reasonably well with the more recent experimental results obtained by Liu and co-workers, who have obtained the NCEs with an improved signal-to-noise ratio and resolution, and observed the non-monotonic change of NCE at low methanol concentration (S. L. Liu et al., private communications).

We are now in a position to analyze the change of the NCEs as a function of the methanol concentration. From eq 2, we can see that three major factors affect the Raman line shape and the NCE (Because of the relatively long vibrational energy relaxation time, the contribution of the $T_1$ term to the line width is only 1.7 cm$^{-1}$. More importantly, the exponential decay affects both the VV and VH components of the spectra, so it would have little influence on the NCE.): (1) the intermolecular vibrational couplings; (2) fluctuations of the vibrational transition energies; (3) the molecule reorientational dynamics.

In pure methanol liquid and at high methanol concentrations, we expect that the strong intermolecular coupling terms dominate the NCEs. To verify this assumption quantitatively, we calculated the NCEs by neglecting the intermolecular coupling terms $\omega_{ij}(t)$ when $i \neq j$, and the results are plotted in Figure 12 as a dashed curve. The NCEs without intermolecular couplings are all smaller than 2 cm$^{-1}$. On the other hand, we have also calculated the NCEs without the reorientational dynamics, by setting $\alpha_{pq}(t)$ in eq 2 to $\alpha_{pq}(0)$. The result is also shown in Figure 12 as a dotted curve, which shows a monotonic change of the NCE as a function of the methanol mole fraction. Thus, we can conclude that the large NCEs at $X_m \geq 0.5$ are indeed caused by the intermolecular couplings, and the decrease of NCE with reduced methanol concentration is consistent with our previous analysis of methanol−methanol hydrogen bonding and intermolecular couplings in Figures 5, 6, and 9. The results in Figure 12 also


dx.doi.org/10.1021/jp300178v | J. Phys. Chem. B 2012, 116, 4543−4551

indicate that the reorientational dynamics could be the main cause of the non-monotonic change of NCEs for $X_m < 0.5$.

Finally, we have calculated the NCE defined by first moments, and the results are shown in Figure 13. The NCE

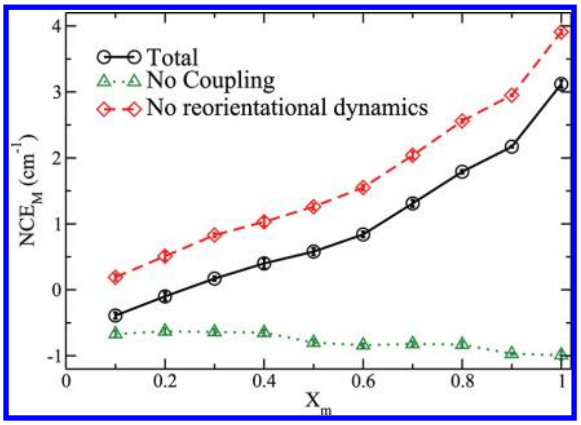


**Figure 13.** Concentration dependence of NCE of CO stretch measured by the first moments in liquid methanol and methanol–water mixtures.

results neglecting intermolecular couplings and reoreintational dynamics were also plotted. As shown in the literature, the first moment definition of the NCE usually gives a better description of the overall couplings between molecules, while the peak position definition will also be sensitive to band asymmetry caused by various reasons such as intermolecular couplings and density fluctuations.[29,69] From Figure 13, we can see that the NCEs defined by first moments are much smaller than those defined by peak positions, which is due to the asymmetric line shape of the Raman peaks. In contrast to the NCE defined by peak positions, the NCE defined by the first moments changes monotonically as the methanol concentration decreases. Again, this is consistent with our previous conclusion that the coupling between CO stretches decreases as the methanol concentration decreases.

In a previous study of the methanol/$CCl_4$ mixture,[29] Musso et al. analyzed the behavior of the CO stretch NCE and related it to the intermolecular vibrational couplings within hydrogen-bonded chains and between chains. A similar analysis also seems to work here based on the above discussion. The difference is that, in the current case, with the addition of water, the intrachain and interchain interactions reduce simultaneously (Figure 9), leading to a monotonic decrease of the NCE defined by the first moment (Figure 13), similar to several other liquid mixtures;[70,71] however, in the case of methanol in $CCl_4$, the interchain couplings reduce much faster and the couplings from directly hydrogen-bonded molecules are dominant in dilute solutions, leading to an increase of the negative NCE defined by first moment.[29]

We now briefly discuss the asymmetric Raman line shapes, which cause the differences between the peak position and first moment definition of the NCE shown in Figures 12 and 13. The band asymmetry parameter $A$ defined in refs 69 and 70 was calculated for the isotropic and anisotropic Raman components and shown in Figure 14

$$A = 2(\Gamma_{blue} - \Gamma_{red})/\Gamma_{full} \quad (12)$$

where $\Gamma_{full}$ is the full width at half-maximum and $\Gamma_{blue}$ and $\Gamma_{red}$ are the blue and red side half width at half-maximum. The

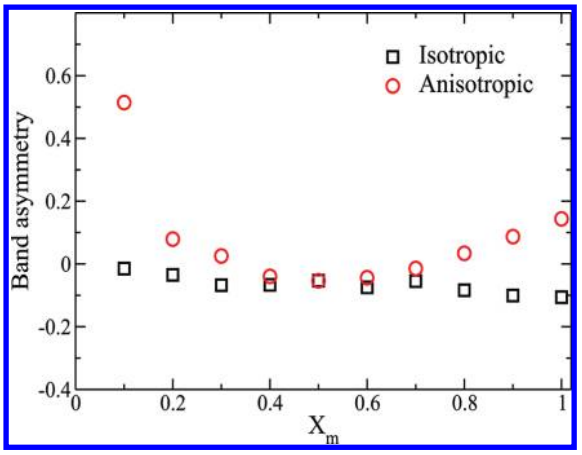


**Figure 14.** Concentration dependence of the asymmetry parameter of the isotropic and anisotropic Raman spectra of CO stretch of methanol in water.

isotropic band asymmetry does not change significantly. For the anisotropic component, the band asymmetry parameter first decreases until $X_m = 0.5$, and increases again at lower methanol concentrations, which is consistent with the non-monotonic change of NCE defined by peak position. In ref 69, the Raman line shape asymmetry of acetone in $CCl_4$ was investigated and ascribed to intermolecular couplings and density fluctuations. We note that these two factors have already been considered in our calculations using the mixed ES/MD dynamics, both in the full calculation and the calculation neglecting the reorientational dynamics. As shown in our calculations, these factors alone are not enough to give the non-monotonic change of NCEs of the CO stretch (dashed and dotted lines in Figure 12), and the reorientational dynamics should play a role in the asymmetry of band shapes and hence the non-monotonic change of NCEs in Figure 12.

On the basis of the above calculations and analysis, the overall picture of the hydrogen-bond structures changes, and its influence on the Raman spectra in methanol–water mixtures is the following: In high methanol concentrations, long methanol chains are destroyed with the addition of water molecules, as methanol–water hydrogen bonds substitute methanol–methanol hydrogen bonds. The consequence of the dilution of methanol in water is that both the positive and negative intermolecular vibrational couplings between methanol molecules are reduced, leading to a reduction of the NCE of CO stretch, since the positive vibrational couplings between C–O oscillators of hydrogen-bonded pairs are the main cause of the negative NCE of C–O stretch. Furthermore, band asymmetry caused by the reorientational dynamics gives rise to an increase of the NCE at low concentrations ($X_m < 0.4$), which results in a non-monotonic dependence of the NCE of CO stretch on the methanol concentration.

## CONCLUSIONS AND DISCUSSIONS

We have calculated the Raman spectra of the CO stretch of liquid methanol and methanol–water mixtures using the combined electronic structure/molecular dynamics method. The vibrational frequencies were obtained from density functional theory calculations and then mapped into an empirical relation to the electrostatic potential at the six atoms of each methanol and three additional sites around the methanol O atom. Vibrational couplings between different


dx.doi.org/10.1021/jp300178v | J. Phys. Chem. B 2012, 116, 4543–4551

molecules were treated with the transition dipole coupling model. The calculated Raman line shapes for pure methanol, and the peak positions as a function of the methanol concentration, agree well with the experimental results.

The change of NCE as a function of the methanol concentration is further analyzed. It is found that, for $X_m > 0.4$, the intermolecular couplings dominate the NCE. The intermolecular couplings between methanol molecules decrease monotonically with the decrease of methanol concentration due to the reduced methanol−methanol hydrogen bonding, which causes the NCE to decrease when more water is added. We also found a slight increase of the NCE from $X_m = 0.4$ to $X_m = 0.3$, which is ascribed to band asymmetry caused by reorientational dynamics. So far, details on how the reorientational dynamics has been changed, and how these changes can be related to liquid structures at different methanol concentrations, are still not very clear (although we note that there has been recent progress in understanding the reorientational dynamics in water[72,73]). These issues will be further studied in revealing the structure and dynamics in different kinds of methanol solutions.

## AUTHOR INFORMATION


### Corresponding Author

*E-mail: qshi@iccas.ac.cn.


### Notes

The authors declare no competing financial interest.

## ACKNOWLEDGMENTS

This work is supported by NSFC (Grant Nos. 20873157 and 20903101), the 973 program (Grant No. 2011CB808502), and the Chinese Academy of Sciences (Grant No. KJCX2.YW.H17 and the Hundred Talents Project).

## REFERENCES


(1) Dougan, L.; Bates, S. P.; Hargreaves, R.; Fox, J. P.; Crain, J.; Finney, J. L.; Reat, V.; Soper, A. K. *J. Chem. Phys.* **2004**, *121*, 6456.

(2) Guo, J.-H.; Luo, Y.; Augustsson, A.; Kashtanov, S.; Rubensson, J.-E.; Shuh, D.; Agren, H.; Nordgren, J. The molecular structure of alcohol-water mixtures. *Phys. Rev. Lett.* **2003**, *91*, 157401.

(3) Dixit, S.; Crain, J.; Poon, W. C. K.; Finney, J. L.; Soper, A. K. *Nature* **2002**, *416*, 829.

(4) Soper, A. K.; Finney, J. L. *Phys. Rev. Lett.* **1993**, *71*, 4346.

(5) Sato, T.; Chiba, A.; Nozaki, R. *J. Chem. Phys.* **1999**, *112*, 2924.

(6) Zerda, T. W.; Thomas, H. D.; Bradley, M.; Jonas, J. *J. Chem. Phys.* **1987**, *86*, 3219.

(7) Lin, K.; Hu, N.; Zhou, X.; Liu, S.; Luo, Y. *J. Raman Spectrosc.* **2012**, *43*, 82.

(8) Zhong, Y.; Warren, G. L.; Patel, S. *J. Comput. Chem.* **2008**, *29*, 1142.

(9) Allison, S. K.; Fox, J. P.; Hargreaves, R.; Bates, S. P. *Phys. Rev. B* **2005**, *71*, 024201.

(10) Fidler, J.; Rodger, P. M. *J. Phys. Chem. B* **1999**, *103*, 7695.

(11) Meng, E. C.; Kollman, P. A. *J. Comput. Chem.* **1996**, *100*, 11460.

(12) Ferrario, M.; Haughney, M.; McDonald, I. R.; Klein, L. M. *J. Chem. Phys.* **1990**, *93*, 5156.

(13) Okazaki, S.; Touhara, H.; Nakanishi, K. *J. Chem. Phys.* **1984**, *81*, 890.

(14) Wilson, K. R.; Cavalleri, M.; Rude, B. S.; Schaller, R. D.; Catalano, T.; Nilsson, A.; Saykally, R. J.; Pettersson, L. G. M. *J. Phys. Chem. B* **2005**, *101*, 10194.

(15) Durov, V. A.; Shilov, I. Y. *J. Mol. Liq.* **2001**, *92*, 165.

(16) Jorgensen, W. L.; Ibrahim, M. *J. Am. Chem. Soc.* **1982**, *104*, 373.

(17) Beggerow, G. *New Series of Landolt-Bornstein*; Springer-Verlag: Berlin, Germany, 1976.

(18) Geiger, A.; Stillinger, F. H.; Rahman, A. *J. Chem. Phys.* **1979**, *70*, 4185.

(19) Yergovich, T.; Swift, G.; Kurata, F. *J. Chem. Eng. Data* **1971**, *16*, 222.

(20) Tsai, J.; Gerstein, M.; Levitt, M. *J. Chem. Phys.* **1996**, *104*, 9417.

(21) Twaki, L. K.; Dlott, D. D. *Chem. Phys. Lett.* **2000**, *321*, 419.

(22) Uemura, T.; Saito, S.; Mizutani, Y.; Tominaga, K. *Mol. Phys.* **2005**, *103*, 37.

(23) Lin, K.; Zhou, X.; Luo, Y.; Liu, S. *J. Phys. Chem. B* **2010**, *114*, 3567.

(24) Dixit, S.; Poon, W. C. K.; Crain, J. *J. Phys.: Condens. Matter* **2000**, *12*, 323.

(25) Kabisch, G.; Pollmer, K. *J. Mol. Struct.* **1982**, *81*, 35.

(26) Ladanyi, B. M.; Liang, Y. Q. *J. Chem. Phys.* **1995**, *103*, 6325.

(27) Shirota, H.; Yoshihara, K.; Smith, N. A.; Lin, S.; Meech, S. R. *Chem. Phys. Lett.* **1997**, *281*, 27.

(28) Giorgini, M. G. Raman noncoincidence effect: A spectroscopic manifestation of the intermolecular vibrational coupling in dipolar molecular liquids. *Pure Appl. Chem.* **2004**, *76*, 157−169.

(29) Musso, M.; Torii, H.; Ottaviani, P.; Asenbaum, A.; Giorgini, M. G. *J. Phys. Chem. A* **2002**, *106*, 10152.

(30) la Cour Jansen, T.; Hayashi, T.; Zhuang, W.; Mukamel, S. Stochastic Liouville equations for hydrogen-bonding fluctuations and their signatures in two-dimensional vibrational spectroscopy of water. *J. Chem. Phys.* **2005**, *123*, 114504.

(31) Torii, H. *J. Phys. Chem. A* **2006**, *110*, 9469.

(32) Auer, B. M.; Skinner, J. L. *J. Chem. Phys.* **2008**, *128*, 224511.

(33) Auer, B. M.; Skinner, J. L. *J. Chem. Phys.* **2008**, *129*, 214705.

(34) Paarmann, A.; Hayashi, T.; Mukamel, S.; Miller, R. Nonlinear response of vibrational excitons: Simulating the two-dimensional infrared spectrum of liquid water. *J. Chem. Phys.* **2009**, *130*, 204110.

(35) Kubo, R. *J. Phys. Soc. Jpn.* **1954**, *9*, 935.

(36) Anderson, P. W. A mathematical model for the norrowing of spectral lines by exchange or motion. *J. Phys. Soc. Jpn.* **1954**, *9*, 316.

(37) Buch, V.; Tarbuck, T.; Richmond, G. L.; Groenzin, H.; Li, I.; Schultz, M. J. Sum frequency generation surface spectra of ice, water, and acid solution investigated by an exciton model. *J. Chem. Phys.* **2007**, *127*, 204710.

(38) Auer, B. M.; Skinner, J. L. *J. Phys. Chem. B* **2009**, *113*, 4125.

(39) Stiopkin, I. V.; Weeraman, C.; Pieniazek, P. A.; Shalhou, F. Y.; Skinner, J. L.; Benderskii, A. V. Hydrogen bonding at the water surface revealed by isotopic dilution spectroscopy. *Nature* **2011**, *474*, 192.

(40) Zheng, R. H.; Sun, Y. Y.; Shi, Q. *Phys. Chem. Chem. Phys.* **2011**, *13*, 2027.

(41) Mukamel, S. *Principles of Nonlinear Optical Spectroscopy*; Oxford: New York, 1995.

(42) Schmidt, J. R.; Roberts, S. T.; Loparo, J. J.; Tokmakoff, A.; Fayer, M. D.; Skinner, J. L. *Chem. Phys.* **2007**, *341*, 143.

(43) Corcelli, S. A.; Lawrence, C. P.; Skinner, J. L. *J. Chem. Phys.* **2004**, *120*, 8107.

(44) Auer, B. M.; Skinner, J. L. *J. Chem. Phys.* **2007**, *127*, 104105.

(45) la Cour Jansen, T.; Zhuang, W.; Mukamel, S. Stochastic Liouville equation simulation of multidimensional vibrational line shapes of trialanine. *J. Chem. Phys.* **2004**, *121*, 10577.

(46) Zhuang, W.; Abramavicius, D.; Hayashi, T.; Mukamel, S. *J. Phys. Chem. B* **2006**, *110*, 3362.

(47) Choi, J.; Lee, H.; Lee, K.; Hahn, S.; Cho, M. *J. Chem. Phys.* **2007**, *126*, 045102.

(48) Gorbunov, R. D.; Nguyen, P. H.; Kobus, M.; Stock, G. *J. Chem. Phys.* **2007**, *126*, 054509.

(49) Logan, D. E. *Chem. Phys.* **1986**, *103*, 215.

(50) Torii, H.; Tasumi, M. *J. Chem. Phys.* **1993**, *99*, 8459.

(51) Torii, H. *J. Phys. Chem. A* **2002**, *106*, 3281.

(52) Buch, V. *J. Phys. Chem. B* **2005**, *109*, 17771.

(53) Krimm, S.; Abe, Y. *Proc. Natl. Acad. Sci. U.S.A.* **1972**, *69*, 2788.

(54) Belch, A.; Rice, S. *J. Chem. Phys.* **1983**, *78*, 4817.

(55) Auer, B. M.; Kumar, R.; Schmidt, J. R.; Skinner, J. L. *Proc. Natl. Acad. Sci. U.S.A.* **2007**, *104*, 14215.

(56) Lin, Y.-S.; Shorb, J. M.; Mukherjee, P.; Zanni, M. T.; Skinner, J. L. Empirical Amide I Vibrational Frequency Map: Application to 2D-IR Line Shapes for Isotope-Edited Membrane Peptide Bundles. *J. Phys. Chem. B* **2009**, *113*, 592−602.
(57) Kwac, K.; Cho, M. *J. Chem. Phys.* **2003**, *119*, 2247.
(58) Oh, K.-I.; Choi, J.-H.; Lee, J. H.; Han, J.-B.; Lee, H.; Cho, M. *J. Chem. Phys.* **2008**, *128*, 154504.
(59) Ham, S.; Kim, J.-H.; Lee, H.; Cho, M. *J. Chem. Phys.* **2003**, *118*, 3491.
(60) Choi, J.; Oh, K.; Cho, M. *J. Chem. Phys.* **2008**, *129*, 174512.
(61) Frisch, M. J.; et al. *Gaussian 03*, revision E.01; Gaussian, Inc.: Pittsburgh, PA, 2004.
(62) Jorgensen, W. L. Development and Testing of the OPLS All-Atom Force Field on Conformational Energetics and Properties of Organic Liquids. *J. Am. Chem. Soc.* **1996**, *118*, 11225−11236.
(63) Smith, W.; Forster, T. R.; Todorov, I. T. *DL_POLY_2*; Daresbury, Warrington: Cheshire, U.K., 2007.
(64) Adams, D. J.; Dubey, G. S. *J. Comput. Phys.* **1987**, *72*, 156.
(65) Allen, M. P.; Tildesley, D. J. *Computer Simulation of Liquids*; Clarendon: Oxford, U.K., 1987.
(66) Luzar, A.; Chandler, D. *Phys. Rev. Lett.* **1996**, *76*, 928.
(67) van den Broek, M. A. F. H.; Nienhuys, H. K.; Bakker, H. J. Vibrational dynamics of the CÂíCO stretch vibration in alcohols. *J. Chem. Phys.* **2001**, *114*, 3182.
(68) The peak width data were read from Figure 7 in ref 28 using a digitizer. The error from our reading should be less than 0.5 $cm^{-1}$.
(69) Musso, M.; Torii, H.; Giorgini, M. G.; Döge, G. *J. Chem. Phys.* **1999**, *110*, 10076.
(70) Musso, M.; Giorgini, M. G.; Döge, G.; Asenbaum, A. *Mol. Phys.* **1997**, *92*, 97.
(71) Musso, M.; Giorgini, M. G.; Torii, H.; Dorka, R.; Schiel, D.; Asenbaum, A.; Keutel, D.; Oehme, K.-L. *J. Mol. Liq.* **2006**, *125*, 115.
(72) Laage, D.; Hynes, J. T. A Molecular Jump Mechanism of Water Reorientation. *Science* **2006**, *311*, 832.
(73) Laage, D.; Hynes, J. T. On the molecular mechanism of mater reorientation. *J. Phys. Chem. B* **2008**, *112*, 14230.